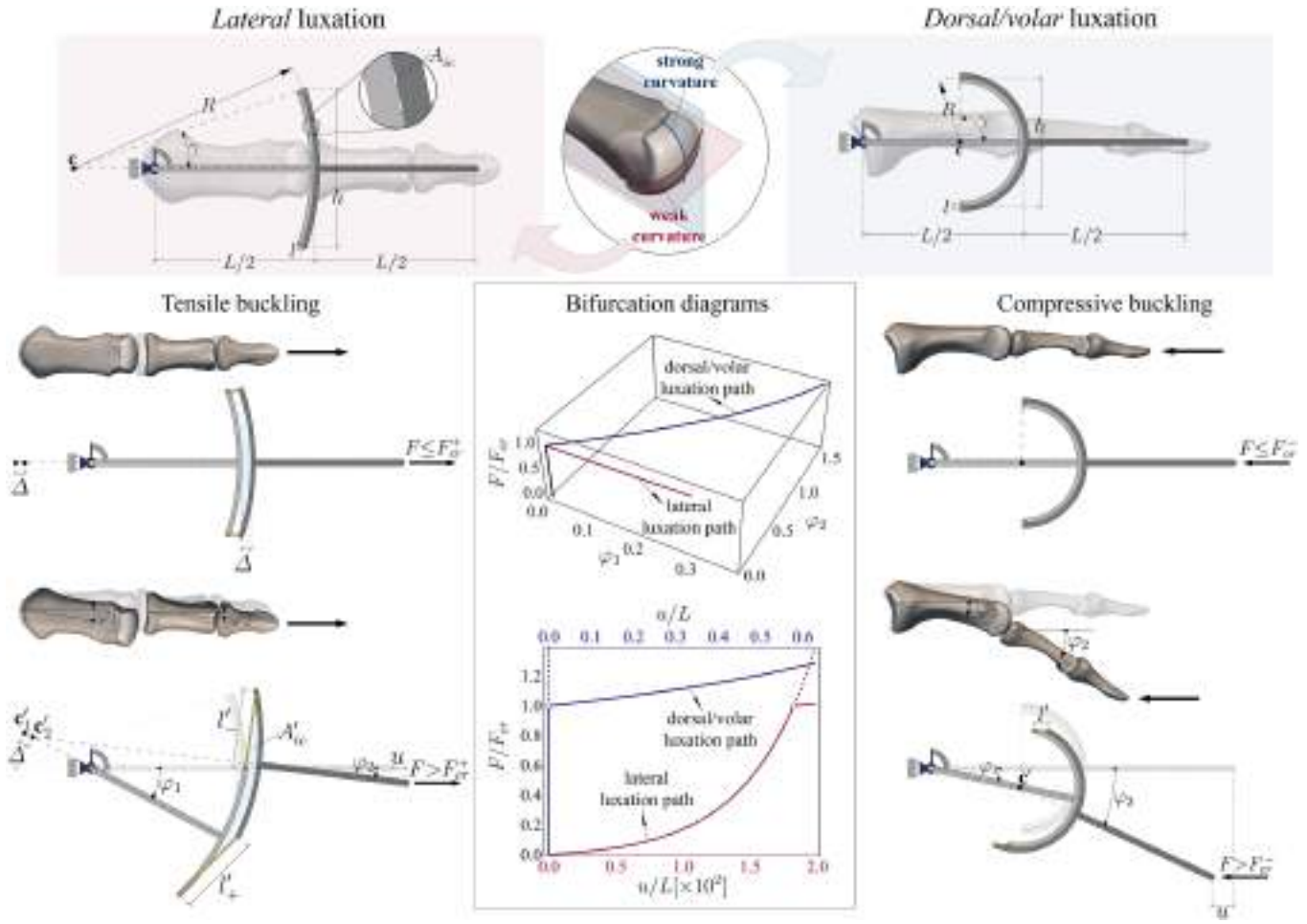

Fig. 3. *Left*: Structural schemes for the tensile-buckling mechanism governing lateral luxations of finger joints: the unloaded and underformed configuration (*Upper* part), an axially distracted configuration under physiological load (*Center*), and a buckled (laterally deviated) state induced by a load overcoming the critical threshold (*Lower* part). *Right*: Sketch of the compressive-buckling mechanism driving finger joints' dorsal/volar luxations: the load-free configuration (*Upper* part), the underformed configuration under physiological load (*Center*), and a buckled (deviated) state induced by an over-critical force (*Lower* part). *Center*: Bifurcation diagrams exhibited by the structural model at growing tensile (red curves; $F_{cr} = F_{cr}^{+}$) and compressive (blue curves; $F_{cr} = F_{cr}^{-}$) load: a 3D plot showing the dimensionless force as a function of the rotation angles (*Upper* part) and the dimensionless force-displacement curve (*Lower* part). Therein, solid tracts identify equilibrium paths followed by the system, while dashed curve portions refer to theoretical unbuckled configurations. Results have been obtained by considering the following values for the geometrical and constitutive parameters: $h = 0.2L$, $s = h$, $l = 0.25L$, $A = 0.1sh$, $\beta = 1$, $t = 0.005L$, $K_{ic} = 0.17E$, $k_r = 0.001EL^3$, with $R = 0.55L$ for the tensile case (lateral luxation) and $R = 0.1L$ for the compressive buckling (dorsal/volar luxation).

can be found by imposing $\partial\Pi/\partial\varphi_1 = \partial\Pi/\partial\varphi_2 = \partial\Pi/\partial\Delta = 0$. In particular, the work done by the force F can be calculated by expressing the magnitude of the horizontal displacement at the right end as

$$u = |\,(R + L/2)\cos\varphi_2 - (R - L/2 - \Delta)\cos\varphi_1 - L|, \quad [9]$$

where $L/2$ is the length of each of the two rigid tracts, so that L is the whole length of the undeformed system, and R is the radius of curvature of the joint, with $R > L/2$ (weak curvature) in the considered anatomical plane. Moreover, the internal elastic energy is provided by the sum of those stored during the deformation inside of the rotational spring at the hinge and of the two bands, both modeled as linear elastic elements, plus the energetic contribution Υ_{ic}. The latter is due to the suction effect resisting distraction, which leads to the development of an intracapsular pulling back pressure in response to increases of the articular volume. More in detail, k_r is the stiffness of the elastic hinge, while E, A, and l are the Young modulus, the nominal cross-sectional area and the length at rest of the bands, respectively, with l accounting for the effective length covered by ligaments in real fingers' articulation. The deformed lengths of the lower and upper bands are l'_+ and l'_-, respectively, and can be calculated as

$$l'_{\pm} = l + \Big\{2R^2\,[1 - \cos(\varphi_1 - \varphi_2)] + \Delta\,\big\{\Delta - 2R\,[\cos\gamma + \cos(\gamma \pm \varphi_1 \mp \varphi_2)]\big\}\Big\}^{1/2}, \quad [10]$$

where γ is the opening angle of the joint, $\gamma = \arcsin(h/2R)$, h being its transverse size. Finally, the energy Υ_{ic} can be expressed as

$$\Upsilon_{ic} = \frac{V_{ic}K_{ic}}{\beta}\Big[e^{\beta(J_{ic}-1)} - 1 - \beta\,(J_{ic} - 1)\Big], \quad [11]$$

obtained by assuming the standard exponential law

$$p_{ic} = \frac{\partial\Upsilon_{ic}}{\partial J_{ic}} = K_{ic}\Big[e^{\beta(J_{ic}-1)} - 1\Big], \quad [12]$$

to describe how the intracapsular pressure p_{ic} varies with the Jacobian of the deformation $J_{ic} = V'_{ic}/V_{ic}$, representing the ratio between the volumes of the articular fluid-filled space in the deformed and undeformed states, approximated as being spatially homogeneous. Here, K_{ic} is the overall bulk modulus of

the synovial fluid and matter inside the intra-articular space, and β is a constitutive parameter ruling the grow rate of the pressure. Moreover, it is possible to consider $V_{ic} = sA_{ic}$ and $V'_{ic} = sA'_{ic}$, where s identifies the out-of-plane size of the joint (remaining invariant during the deformation process), while A_{ic} and A'_{ic} are the areas occupied by the projection of the intracapsular domain onto the horizontal anatomical plane at the reference and current configurations of the system, respectively. As sketched in Fig. 3, the reference area can be estimated as $A_{ic} \approx ht$, where t is a nominal thickness, while geometrical considerations allow to obtain the following form for the current area A'_{ic}:

$$A'_{ic} = A_{ic} + R\Delta\left[1 + \cos\left(\varphi_1 - \varphi_2\right)\right]\sin\gamma. \qquad [13]$$

The above equations led to a numerical solution, with the aid of the software Mathematica®. The diagrams reported in Fig. 3 (red curves) show how, due to the cooperation of the elasticity of the ligaments and the suction associated with the intracapsular pressure, the bifurcation tensile load F_{cr}^{+} is attained at the end of an initial deformation process connected with the axial distraction of the bone segments and is followed by a significant reduction in the force gradient with respect to the end displacement, when the post-buckling phase evolves. This mechanical behavior demonstrates how, in case of high distracting loads, tensile buckling rules lateral luxation and provides an overall stress shielding by deviating fingers from their natural straight configuration.

Dorsal/volar Luxations Ruled by Compressive Buckling along the Strong Curvature. Dorsal and volar luxations of fingers are injuries complementary to lateral ones and occur in response to high compressive actions. In this case, the digits dislocate in the sagittal plane of the hand, where articular joints exhibit strong curvatures. From a mechanical point of view, these injuries can again be interpreted as elastic instabilities, which lead the bone-joint-bone system to deviate its configuration at the onset of compressive buckling as shown in the Fig. 3, *Right*. In more detail, the mechanics of dorsal/volar luxations can be treated by following an approach analogous to that employed for lateral ones. However, in this case, the rotations φ_1 and φ_2 are the sole Lagrangian variables needed for a complete description of the kinematics of the system, as no separation at the joint interface occurs under compression. As a consequence, the total potential energy in Eq. **8** lacks now the energy term Υ_{ic}, and the expressions for the displacement u in Eq. **9** and the lengths of the two elastic ligaments $l'_{\pm}$ in Eq. **10** simplify by imposing $\Delta = 0$.

Stationarity of Π allows to find the equilibrium bifurcation diagrams shown in Fig. 3 (blue curves) and the critical compressive load can be obtained in closed-form as

$$F_{cr}^{-} = \frac{\sqrt{a_1^2 + 4a_0a_2} - a_1}{2a_0}, \qquad [14]$$

the coefficients a_0, a_1, and a_2 being:

$$\begin{aligned} a_0 &= l\left(4R^2 - L^2\right), \\ a_1 &= 2\left[k_r l\left(2R + L\right) + 4EAR^2L\right], \\ a_2 &= 8EAk_rR^2, \end{aligned} \qquad [15]$$

with $R < L/2$ (strong curvature) and $a_1^2 + 4a_0a_2 \geq 0$. It is worth noticing that the critical value in Eq. **14** corresponds to the minimum between two possible bifurcation loads.

Similarly to the lateral luxation (governed by tensile buckling), the mechanical model demonstrates that dorsal/volar dislocations, ruled by compressive elastic instability, provide again stress shielding of the bone-joint-bone finger system in the sagittal plane where digits are deviated, invited by the strong curvature of the articulating bone segments' heads (see bifurcation diagrams in Fig. 3).

An Experimental Proof of Concept Prototype. The proposed luxation mechanism has been validated by an experimental proof of concept model, based on a 3D-printed prototype, incorporating the suction effect due to the articular capsule and a design of the elastic ligaments tailored to replicate the real functioning of the fingers' bone-joint-bone system, as reported in Fig. 4. Laboratory uni-axial tests performed on the built-up prototype have confirmed that both compressive and tensile buckling modes can be reproduced if all the main geometrical and mechanical features characterizing the articulation are taken into account. In particular, under compression, instability-induced deviation of the system's tracts from the straight configuration occurs in the strong curvature plane, as it happens for dorsal and volar dislocations, while bifurcation associated with tension takes place in the weak curvature plane, after an initial phase of axial distraction, similarly to lateral dislocations. These pieces of evidence support the theoretical model and contribute to experimentally highlight the double capability of finger joints to undergo both compressive and tensile buckling, so providing luxation as a stress-shielding strategy.

Discussion and Conclusion

The main conclusion of the present study is that dislocations—common injuries of bone articulations as finger joints—can be interpreted through an unprecedented mechanical instability phenomenon that unifies compressive and tensile buckling and leads to recognize luxation as a protection mechanism from more severe damage for bones, exposed to extreme load. This is related to the characteristic double-curvature geometry of the bones' epiphyses at the joints, allowing for a two-mode (lateral and dorsal/volar) fingers' dislocation model, which has theoretically and experimentally demonstrated to be the result of a unique optimized design by nature. The latter ensures stress shielding under axial forces exceeding physiological limits, independently from their sign. In tension, the proposed mechanism provides a hallmark example of tensile critical load involved in functioning of a natural system.

The outcomes of the present research can be used in the design of bio-inspired, mechanically and geometrically optimized joints and structures, which can find a number of applications at different scales, from soft- and micro-robotics to active and passive actuators and exoskeletons in healthcare for rehabilitation purposes.

Materials and Methods

The proof of principle prototype of the fingers' bone-joint-bone system was manufactured through 3D printing and tested under both tensile and compressive forces. A double-curvature joint was designed to replicate (scale 3:1) the two complementary curvatures exhibited by the finger bones' epiphyses in a 3D printed model realized with STRATASYS F170 and STRATASYS Object30 printers, using polymeric materials (ABS - Acrylonitrile Butadiene Styrene) for the bone tracts and a resinous material for the joint elements, Fig. 4. Particular attention was devoted to mimic both the lubrication related to the synovial fluid and the suction effect occurring within the articular capsule. To the purpose, a film of high-pressure resistant grease (NLGI 3 lithium by AREXONS) was interposed between the two contact surfaces of the joined elements and an intact portion of sow intestine was used to encapsulate the joint. Finally, elastic

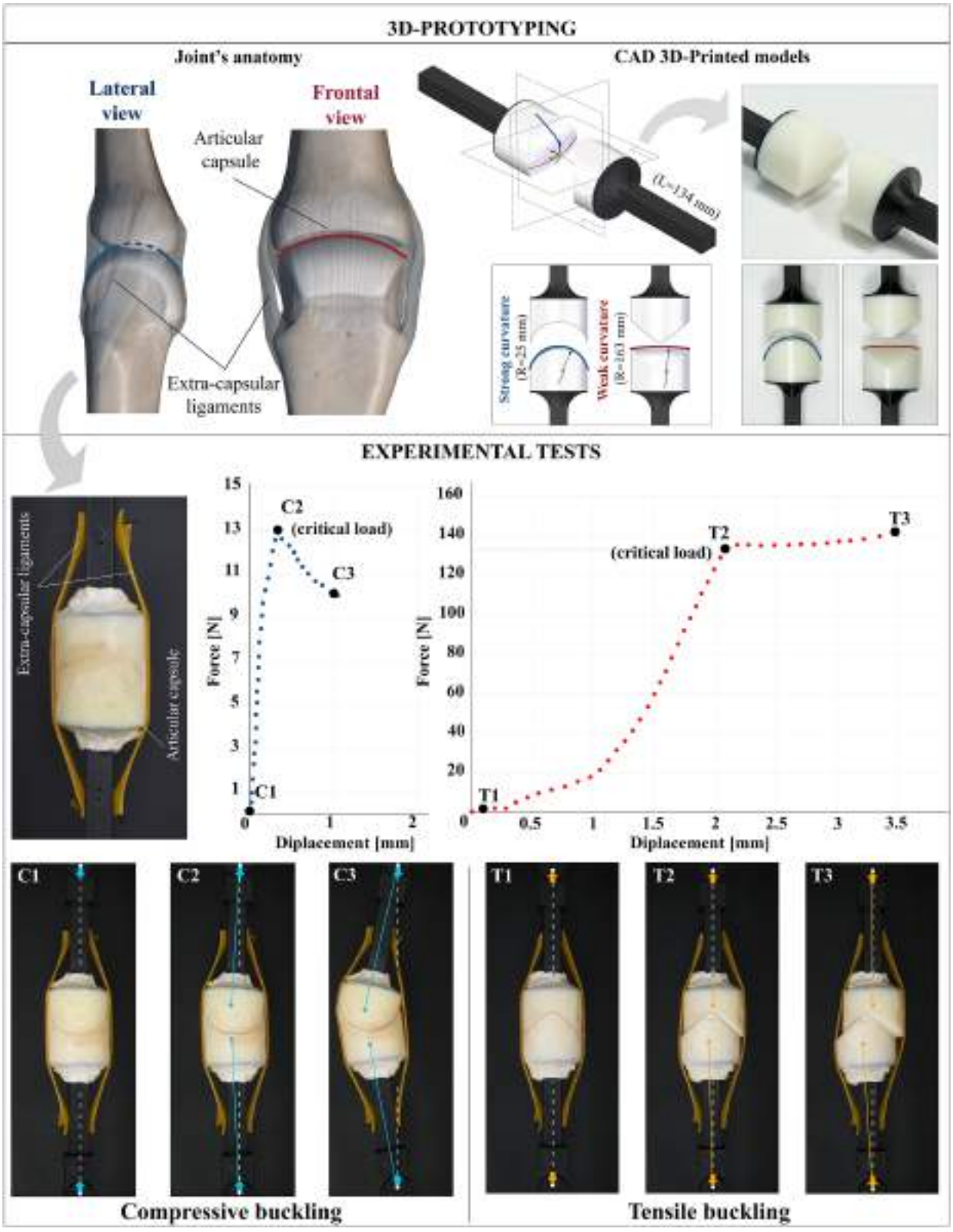

Fig. 4. *Upper part*: Lateral and frontal views of the fingers' joint anatomy pointing out the two characteristic (strong and weak) curvatures of the articulating bone terminals (*Left*) are compared with the CAD model and 3D-printed prototype of the finger bone-joint-bone system (*Right*). *Central part:* Assembled prototype employed for experimental tests—equipped with an articular capsule obtained from sow intestine, lubricating grease at the joint interface and ligament-like elastic bands—(*Left*) produces the compressive (blue) and tensile (red) force-displacement curves (*Right*). *Lower part:* Sequences of images showing the buckling kinematics exhibited by the system during the compressive (frames C1–C3) and tensile (frames T1–T3) tests; in particular, frames C1 and T1 correspond to initial (unloaded and undeformed) configurations, frames C2 and T2 show states immediately following the onset of equilibrium bifurcation and frames C3 and T3 provide configurations reached in the post-buckling phase. It is worth noticing that, due to the partial compressibility of the grease layer at the interface, the response in compression does not recover the infinitely rigid behavior theoretically predicted. Also, consistently with the anatomy of the finger joints and the theoretical model, elastic bands were positioned laterally in the sagittal and frontal planes and are shown in the photos deformed under compression or tension.

bands were fixed on the sides of the assembled structure in order to simulate the presence of extracapsular ligaments, as illustrated in Fig. 4. The mechanical response of the prototype was measured by employing a electromechanical biaxial testing machine (ElectroForce TestBench four linear motors Planar Biaxial 230*V* with integrated 200*N* load-cells by TA Instruments) used in a uniaxial mode to reproduce both tensile and compressive loading conditions. Specifically, a progressively increasing axial displacement was quasi-statically (at a velocity of 0.05 mm/s) applied to the ends of the structure, both constrained through 3D printed hinges. The reaction forces on the supports were measured via the above-specified 200*N* load cells.

Data, Materials, and Software Availability. All study data are included in the main text.

ACKNOWLEDGMENTS. We acknowledge the financial support from the European Research Council under the European Union's Horizon 2020 research and innovation programme, Grant agreement No. ERC-ADG-2021-101052956-BEYOND. M.F., S.P., A.C., and A.R.C. also acknowledge the support by the Italian Ministry of University and Research, under the complementary actions to the National Recovery and Resilience Plan "Fit4MedRob - Fit for Medical Robotics" Grant (# PNC0000007).

1. H. Gray, *Anatomy of the Human Body* (Philadelphia Lea and Febiger, ed. 20, 1918).
2. M. Brocato, P. Podio-Guidugli, A bone-wise approach for modeling the human hind-midfoot. Part i: Kinematics. *Meccanica* **57**, 977–998 (2022).
3. J. Gray, *How Animals Move* (Cambridge University Press, 1953).
4. J. Ralphs, M. Benjamin, The joint capsule: Structure, composition, ageing and disease. *J. Anat.* **184**, 503 (1994).
5. V. C. Mow, G. A. Ateshian, R. L. Spilker, Biomechanics of diarthrodial joints: A review of twenty years of progress. *J. Biomech. Eng.* **115**, 460–467 (1993).
6. J. Mech, A. Neville, A. Morina, T. Liskiewicz, Y. Yan, Synovial joint lubrication-does nature teach more effective engineering lubrication strategies? *Proc. Inst. Mech. Eng. Part C Eng. Sci.* **221**, 1223–1230 (2007).
7. S. C. Cowin, S. B. Doty, *Tissue Mechanics* (Springer, 2007).
8. Yc. Fung, *Biomechanics: Mechanical Properties of Living Tissues* (Springer Science & Business Media, 2013).
9. W. C. Hung, C. H. Chang, A. T. Hsu, H. T. Lin, The role of negative intra-articular pressure in stabilizing the metacarpophalangeal joint. *J. Mech. Med. Biol.* **13**, 1350049 (2013).
10. W. Inokuchi, B. S. Olsen, J. O. Søjbjerg, O. Sneppen, The relation between the position of the glenohumeral joint and the intraarticular pressure: An experimental study. *J. Shoulder Elbow Surgery* **6**, 144–149 (1997).
11. G. N. Kawchuk *et al*., Real-time visualization of joint cavitation. *PloS One* **10**, e0119470 (2015).
12. P. Habermeyer, U. Schuller, E. Wiedemann, The intra-articular pressure of the shoulder: An experimental study on the role of the glenoid labrum in stabilizing the joint. *Arthrosc.: J. Arthrosc. Related Surgery* **8**, 166–172 (1992).
13. T. D. Gibb, J. A. Sidles, D. Harryman 2nd, K. J. McQuade, F. Matsen 3rd, The effect of capsular venting on glenohumeral laxity. *Clin. Orthopaed. Related Res.* **268**, 120–127 (1991).
14. S. Alexander, D. F. Southgate, A. M. Bull, A. L. Wallace, The role of negative intraarticular pressure and the long head of biceps tendon on passive stability of the glenohumeral joint. *J. Shoulder Elbow Surg.* **22**, 94–101 (2013).
15. N. Sharma, M. Venkadesan, Finger stability in precision grips. *Proc. Natl. Acad. Sci. U.S.A.* **119**, e2122903119 (2022).
16. D. Ramponi, M. J. Cerepani, Finger proximal interphalangeal joint dislocation. *Adv. Emer. Nursing J.* **37**, 252–257 (2015).
17. R. B. Prucz, J. B. Friedrich, Finger joint injuries. *Clin. Sports Med.* **34**, 99–116 (2015). Sports Hand and Wrist Injuries.
18. N. Sundaram, J. Bosley, G. S. Stacy, Conventional radiographic evaluation of athletic injuries to the hand. *Radiol. Clin. North Am.* **51**, 239–255 (2013). Imaging of Athletic Injuries of the Upper Extremity.
19. K. E. Elzinga, K. C. Chung, Finger injuries in football and rugby. *Hand Clin.* **33**, 149–160 (2017).
20. L. Laver *et al*., *Basketball Sports Medicine and Science* (Springer, 2020).
21. A. W. Bach, Finger joint injuries in active patients: Pointers for acute and late-phase management. *Phys. Sportsmed.* **27**, 89–104 (1999).
22. A. J. Logan, N. Makwana, G. Mason, J. Dias, Acute hand and wrist injuries in experienced rock climbers. *British J. Sports Med.* **38**, 545–548 (2004).
23. S. Gnecchi *et al*., "Hand and finger injuries in rock climbers" (Tech. Rep., Springer, 2015).
24. D. Zaccaria, D. Bigoni, G. Noselli, D. Misseroni, Structures buckling under tensile dead load. *Proc. R. Soc. A: Math. Phys. Eng. Sci.* **467**, 1686–1700 (2011).
25. S. P. Timoshenko, J. M. Gere, *Theory of Elastic Stability* (McGraw-Hill, 1961).
26. D. Bigoni, *Nonlinear Solid Mechanics - Bifurcation Theory and Material Instability* (Cambridge University Press, 2012).
27. S. Palumbo, L. Deseri, D. R. Owen, M. Fraldi, Disarrangements and instabilities in augmented one-dimensional hyperelasticity. *Proc. R. Soc. A: Math. Phys. Eng. Sci.* **474**, 20180312 (2018).
28. M. Fraldi, S. Palumbo, A. Cutolo, A. R. Carotenuto, F. Guarracino, On the equilibrium bifurcation of axially deformable holonomic systems: Solution of a long-standing enigma. *Proc. R. Soc. A: Math. Phys. Eng. Sci.* **477**, 20210327 (2021).
29. C. Siviy *et al*., Opportunities and challenges in the development of exoskeletons for locomotor assistance. *Nat. Biomed. Eng.* **7**, 456–472 (2022).
30. D. Misseroni, G. Noselli, D. Zaccaria, D. Bigoni, The deformation of an elastic rod with a clamp sliding along a smooth and curved profile. *Int. J. Solids Struct.* **69–70**, 491–497 (2015).
31. D. Hu, D. Howard, L. Ren, Biomechanical analysis of the human finger extensor mechanism during isometric pressing. *PloS One* **9**, e94533 (2014).
32. D. Bigoni, N. Bordignon, A. Piccolroaz, S. Stupkiewicz, Bifurcation of elastic solids with sliding interfaces. *Proc. R. Soc. A: Math. Phys. Eng. Sci.* **474**, 20170681 (2018).